THE CHALK RIVER SUPERCONDUCTING CYCLOTRON

J.H. Ormrod*, C.B. Bigham*, K.C. Chan†, E.A. Heighway*
C.R. Hoffmann*, J.A. Hulbert*, H.R. Schneider* and Q.A. Walker*

ABSTRACT

The Chalk River K=520, 4-sector, superconducting cyclotron[1], is designed to accelerate all ions from Li (to 50 MeV/u) to U (to 10 MeV/u) using a 13 MV tandem as injector. Concurrent with the design of the integrated accelerator facility we have been testing major components - specifically the radiofrequency accelerating structure and the cyclotron magnet. The project has now been approved and site preparation is underway. This paper reports on the cyclotron assembly, initial cooldown of the cryostat and first magnetic field measurements.

RADIOFREQUENCY ACCELERATING SYSTEM

Initial tests of the radiofrequency accelerating system have begun and are described in detail elsewhere in these proceedings[2]. At present, the accelerating structure is housed in a temporary vacuum jacket but will be transferred to the magnet when magnetic field mapping is complete. The frequency range of 31-62 MHz has been demonstrated at low power with the critically coupled Q in the range 1600 to 2300. Tests at 50 MHz and 15 kW have achieved about half the nominal 100 kV accelerating voltage.

ASSEMBLY OF THE MAGNET

Figure 1 shows the major magnet components, the cryostat, yoke walls, poles, hill assembly and end-rings.

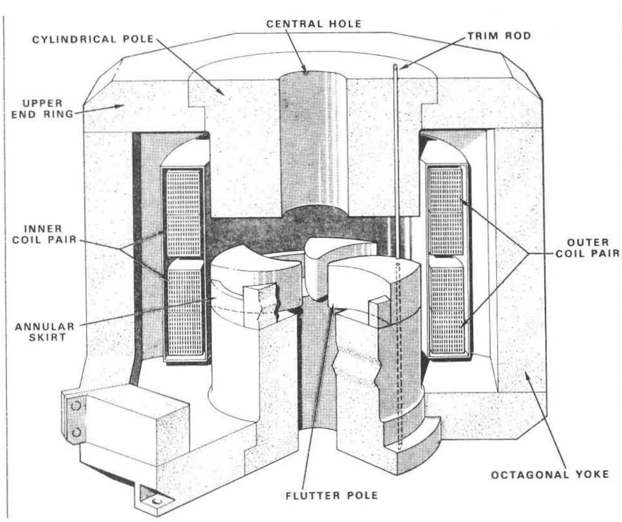

Fig. 1 Simplified cutaway view of the magnet assembly. The top flutter pole assembly has been omitted for clarity.

The magnet was first completely assembled without the cryostat to measure the hill alignment and separation. Near the outside edge, the separation is uniform to better than 0.05 mm and within 0.1 mm of the nominal value of 40 mm. The hill dimensions are everywhere within 0.1 mm of the design values and for the most part considerably better.

To allow access to the cyclotron midplane the bottom pole is lowered on four jack screws. On seating, the pole is aligned by linear bearings that reposition the pole to within 0.05 mm.

The 104 trim rod holes bored through the poles are all within 0.12 mm of the design position at the midplane surface. (For the initial tests, only 3 of these holes were bored in each hill.)

All dimensions of the magnet assembly are within the required tolerances[3].

Figure 2 is a cutaway drawing of the cryostat showing the coils, helium cans and midplane bridge structure.

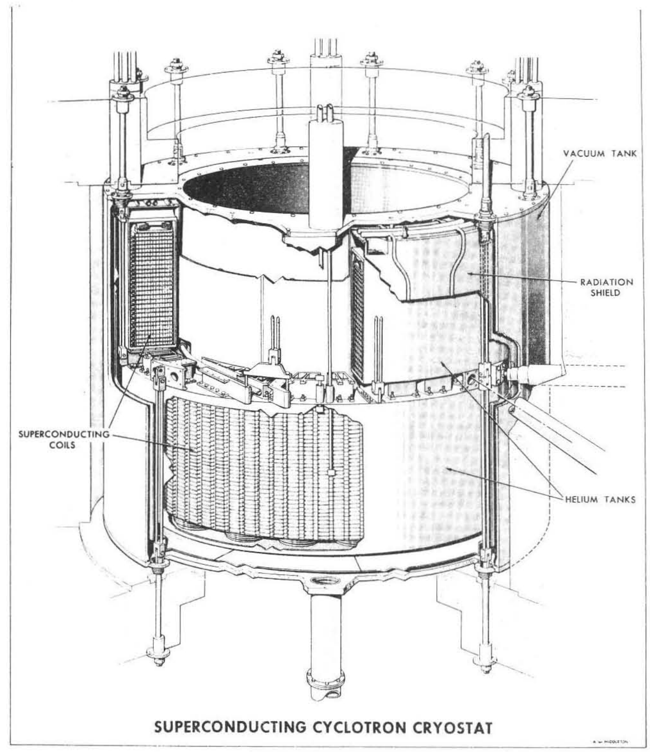

Fig. 2 Cutaway drawing of the cryostat.

The coil consists of 32 double pancakes. The magnetic centre of each double pancake was positioned within 0.1 mm of the coil axis by passing a current through the pancake and using the magnetic field gradient near its inner edge. A central post defined the axis of the coil and a rotating arm centred on this post spanned the diameter of the coil. Two bucking pick-up coils, one at each end of the arm, gave a sensitive means of measuring the displacement of the pancake's magnetic centre. An array of Belleville springs on the top and bottom of the coil assembly was precompressed before welding the stainless steel helium can around the coils. The springs then maintain an axial live loading of the coils onto the bridge structure. Figure 3 is a photograph of the assembled coil before the outer wall of the upper helium can was welded into place and shows the suspension points on the bridge and the Belleville spring assemblies at the top of the upper coil.

* Accelerator Physics Branch, Atomic Energy of Canada Limited, Physics Division, Chalk River Nuclear Laboratories, Chalk River, Ontario, Canada.

† Present address: Atomic Energy of Canada Limited, Whiteshell Nuclear Research Establishment, Pinawa, Manitoba, Canada.

0018-9499/79/0400-2034$00.75 © 1979 IEEE

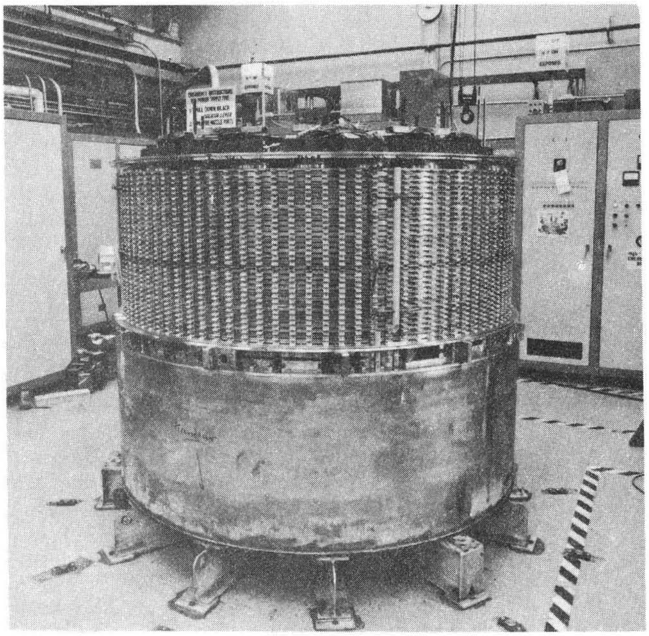

Fig. 3 The assembled coil before the outer wall of the upper helium can was welded into place.

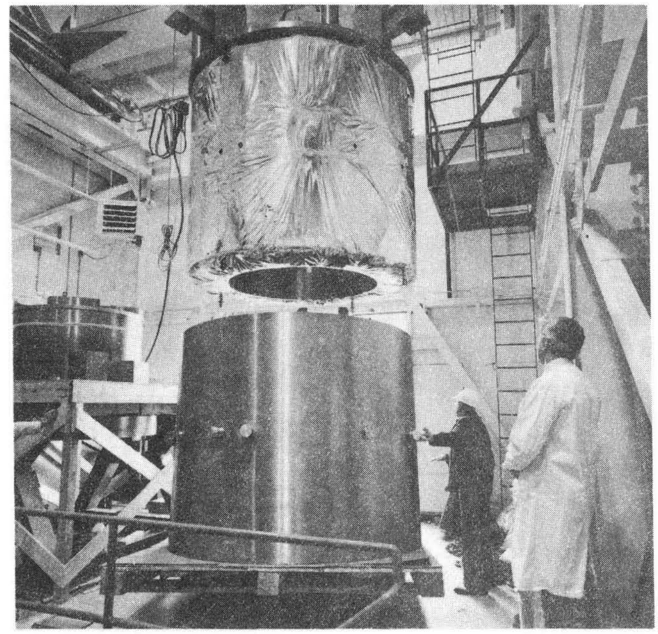

Fig. 4 The coil assembly, wrapped in super insulation, suspended from the upper ring of the vacuum vessel being lowered into the outer wall. The inner wall is already attached and is visible inside the coil. The inverted upper pole is visible at the left.

The welded helium can assembly is wrapped with several layers of super insulation and completely enclosed by a segmented copper radiation shield which in turn is wrapped with several layers of super insulation and enclosed by the stainless steel cryostat vacuum vessel. The coil is suspended by 12 pairs of 9.5 mm diameter titanium rods attached to the bridge. Four similar pairs of rods pull downwards on the bridge structure and 8 individual rods attached radially are used for positioning and holding the coil in the centre. During assembly the coil hangs from the top plate of the cryostat vacuum vessel, but when the cryostat is installed in the yoke, the load is transferred to the upper end ring of the yoke. The lower axial bracing and radial bracing also react against the yoke.

Figure 4 shows the coil assembly wrapped in super insulation being lowered into the outer wall of the cryostat vacuum vessel. The injection, extraction and probe vacuum penetrations through the bridge structure were omitted on this assembly; they will be installed when the radiofrequency accelerating structure is added.

Figure 5 shows the 30 tonne upper end ring of the yoke being lowered into position over the four cryostat towers. At this stage the coil was suspended from the upper ring of the cryostat vacuum vessel by 12 nuts bearing on the clevis pins visible around the outside edge of the cryostat. Two of the 8 radial bracing rods are visible extending through the yoke wall at the lower right of the photograph. The 300 mm diameter extraction hole is visible at the lower left-hand side of the photograph.

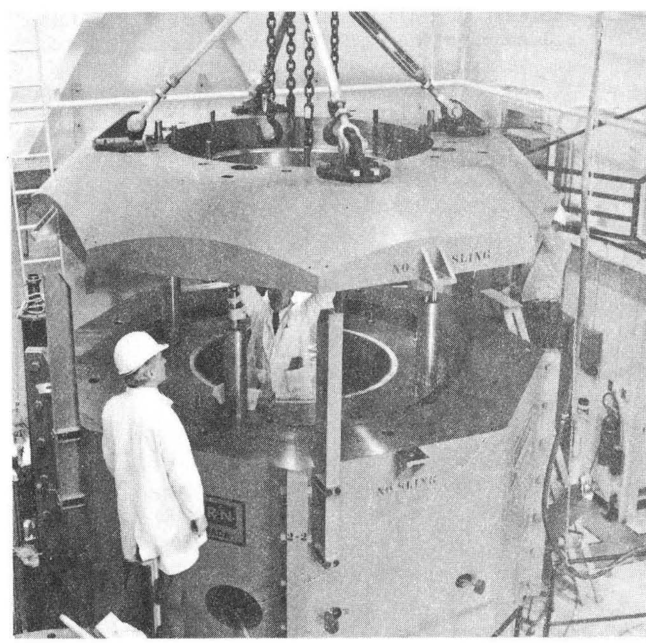

Fig. 5 The 30 tonne upper end ring being lowered over the four cryostat towers onto the yoke.

OPERATION

The cryostat vacuum vessel is pumped with a 150 mm oil diffusion pump through one of the bottom tower holes. The initial vacuum of several times 10^{-5} torr fell to approximately 1×10^{-6} torr when the helium cans were filled with liquid. Initial problems with vacuum leaks from cold O-rings on the towers that house the current leads were overcome by adding trace heating and eventually installing teflon O-rings. With the helium cans approximately half full of liquid, the gate valve to the diffusion pump was closed and the cryostat vacuum rose from 1.4×10^{-6} torr to 3.3×10^{-6} torr air equivalent in 2-1/2 hours. Assuming this increase is due only to helium leaking from the coil cans, the corrected leak rate is 2×10^{-6} torr ℓ/s. This leak may be accounted for by a known perforation of a bellows assembly.

Figure 6 is a schematic of the cryostat, dewar and liquefier. Transfer tubes A and D have three segments for assembly purposes, H and J two. Transfer tube D, the longest at 11.5 m, is valved and is used to carry liquid to or from the cryostat, A carries cold gas (and eventually liquid) to the cryostat, H returns the cold gas to the liquefier and J carries gas at approximately 80°K to the radiation shield. With the cryostat cold and a flow of 11 m^3/hr through J, the average temperature from the thermocouples distributed around the shield was ∿ 130°K.

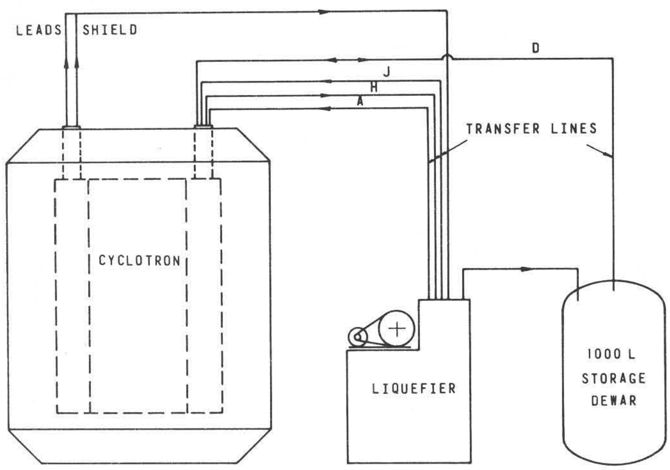

Fig. 6 Schematic of the cryogenic system.

Nineteen thermocouples are distributed throughout the coil to monitor the temperature. There are voltage taps on the 32 double pancakes to monitor the coil during excitation. A small current (normally 2 amps) was passed through the coil during the cooldown and these taps were used to monitor the average pancake temperatures using the known relationship between temperature and resistivity of the copper. This diagnostic is good down to about 15°K and is the one displayed in Fig. 7 that shows the cooldown for the top and bottom pancakes and the one immediately below the bridge.

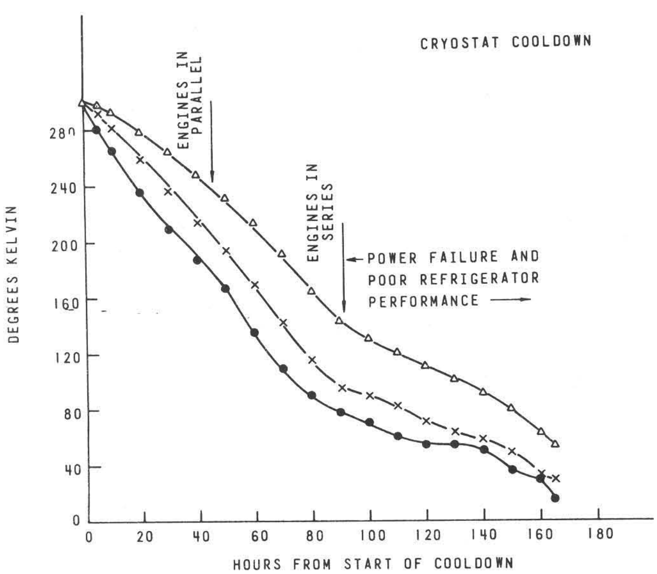

Fig. 7 Cryostat cooldown. The top curve is the average temperature of the uppermost double pancake, the middle curve of the pancake immediately below the bridge and the bottom curve of the lowermost pancake.

The helium boil-off rate was more than twice the calculated value. It was ∿ 45 ℓ/h when full with 660 litres decreasing to ∿ 11 ℓ/h with 100 litres. This higher boil-off is attributed to a heat leak between the bridge and radiation shield and to excessive superficial losses - especially on the inner wall of the cryostat where small clearances between the helium can and the radiation shield limit the number of layers of super insulation. More layers of super insulation will be applied during the upcoming rewrap by using fibre glass-paper separators rather than Dimplar. The high boil-off rate reduced operating times to the order of an hour, which was quite adequate to obtain a 360° field map.

The inner half of the coil (16 double pancakes nearest the midplane) is excited by one channel of a dual power supply and the outer half by the other. During charging the two channels operate in a master-slave relationship with the master supply voltage maintained constant at a preselected value, while the slave supply voltage is automatically adjusted to achieve equal charging rates. When the current set point for either coil pair is reached, the corresponding supply automatically switches to current regulation mode and the other supply switches to, or remains in voltage control mode until it reaches its set point. After some initial problems were corrected, the supplies have operated well; when delivering 1700 A each, the measured current in the difference lead was ± 18 mA.

The inductance of the whole winding at low currents is of the order of 200 H and at higher currents reduces to 3.4 H for the inner coil and 2.6 H for the outer coil, with a mutual inductance of 1.9 H; all within 5% of the calculated values.

Six transducers monitor the heights of the Belleville springs that compress the coil onto the bridge structure. These springs were designed to maintain an approximately constant force of 140 kN over a range of 2.5 mm then reduce to zero over the next 2 mm. The springs relaxed approximately 1 mm on cooling the coil to 4.5 K. As the coil was excited the magnetic loading further compressed the coil another 1.8 mm, of which 0.7 mm was inelastic as the coil bedded down.

Maintenance of the superconducting state in the coil was monitored with voltage taps on each double pancake winding. The taps on pancakes symmetrically located above and below the midplane were paired in opposition. The difference voltages were monitored with a scanning voltmeter. No significant voltages were detected even when the liquid level was allowed to fall below the upper two double pancakes.

Transient behaviour of the coil was monitored by recording the two difference voltages between the upper and lower coils of both the inner and outer pairs (see Fig. 1) with a chart recorder. During initial charging of the coil the difference voltage traces showed numerous small spikes (10 mV amplitude). These spikes did not appear on subsequent coil excitations and were probably due to small conductor motion as the coil tightened. On discharging, several spikes approximately 10 mV in amplitude were observed when the current was < 10% of full excitation. Simultaneous spikes were observed on a separate dB/dt monitor. Whether these spikes result from stress relieving in the coil or in the iron yoke has not been determined.

At full excitation, the attractive force on the pole is 10 MN. The reduction in the midplane gap was monitored by a transducer; at 75% of full attractive force, the 40 mm gap closed by 0.40 mm, approximately 20% greater than expected. The gap monitor limited the field measuring equipment to 90° azimuth scan and was removed to permit full 360° field maps to better centre the coil before going to higher excitations.

Originally, it was planned to centre the coil with the strain gauges on the radial bracing. The coil appeared to be weakly decentering but the reproducibility of the strain gauge readings was inadequate to give an accurate placement, so the characteristic first harmonic "thumb-print" of the coil was used to centre the coil. The initial position was 1.4 mm off-centre and the first adjustment reduced this to 0.2 mm where it remained for the rest of the tests.

Each of the three current leads[4] is a 10 mm diameter 800 mm long solid copper bar with 264 copper washers, 25.4 mm O.D. brazed along its length. A Kapton and fibreglass sleeve is wrapped around the washers and boil-off gas flows up through staggered slots in the washers to cool the lead. All leads were tested to 2600 A before assembly following development tests to 3300 A. Magnet tests were halted when one of the lead cooling channels became partially obstructed.

The vacuum cryostat is now being disassembled to improve the insulation and modify the radiation shield near the bridge to reduce the boil-off rate. The repair of the current lead is a relatively minor operation once the cryostat is dismantled. The cryostat will be dismantled again after field mapping is complete to install the midplane penetrations and the radiofrequency accelerating structure.

MAGNETIC FIELD MEASURING APPARATUS

The magnetic field was measured by 40 flip coils mounted on a perspex rod that extended along a radius at the midplane of the cyclotron. The perspex rod can be rotated through 180° (flipped) by a pneumatic drive. The arm is moved azimuthally by a stepping motor drive assembly and the position is read by an optical encoder with an accuracy of 0.02°. The system is operated and the data collected by a PDP 11/34 computer (operating under MUMTI, Multi User Multi Task Interpreter)[5] using one crate of the serial CAMAC highway.

The flip coils have approximately 1,150 turns of No. 38 copper wire, layer-wound on a MACOR bobbin 6.12 mm high and diameter 4.17 mm resulting in a coil O.D. of 8.7 mm to minimize errors in gradient fields[6]. The integrators were patterned after those of Mosko et al[7]. Each coil integrator assembly was calibrated in magnetic fields up to 1 T against an NMR probe and had a sensitivity of approximately 1.3 volts per Tesla.

The magnetic field at a given azimuth was measured by the following sequence:

1. short circuit integrator inputs and wait 3 seconds
2. scan 40 integrators (∿ 4 seconds)
3. flip arm (∿ 3 seconds)
4. scan integrators (∿ 4 seconds)
5. return arm (∿ 3 seconds)
6. scan integrators (∿ 4 seconds)
7. advance arm 2° (∿ 3 seconds)
8. scan integrators (∿ 4 seconds).

The readings were corrected for integrator drift by subtracting the average of the readings taken at steps 2 and 6 from those at step 4. This procedure requires approximately 100 minutes to complete a 360° map. A faster procedure requiring only 44 minutes for a complete map is to flip the arm at 10° intervals and repeat only steps 7 and 8 at the intervening 4 angles then calculate the intermediate points from the field differences. The latter method was used for most of the results reported here.

MAGNETIC FIELD MEASUREMENTS

Figure 8 compares the measured and calculated azimuthally averaged magnetic fields for three excitations which approximately span the proposed cyclotron operating range. The octagonal yoke walls are represented by an equivalent cylindrical shell in a TRIM[8] calculation, while the flutter poles are represented as being uniformly magnetized ($\mu_o M$ = 2.14 T) in an equivalent current sheet calculation. Effects of the holes in the yoke as well as the eighty trim rods absent from the pole are included in the calculation. The currents used for the calculations were those set on the power supply DAC's.

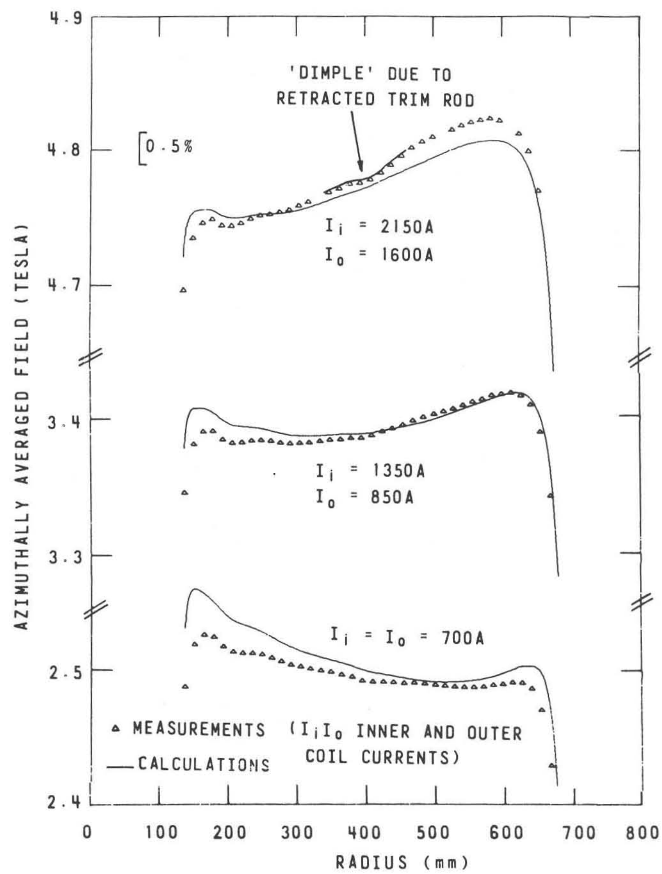

Fig. 8 Comparison of measured and calculated azimuthally averaged magnetic fields for three excitations which approximately span the cyclotron operating range.

The agreement of the calculated and measured fields is good with an rms deviation of 0.26% at an average field <B> of 4.8 T, 0.31% at 3.4 T and 0.72% at 2.5 T. General features are the trend to a larger measured field slope, d<B>/dr, than calculated and slower fall off of the field at the inner and outer field edges. The latter will influence injection and extraction by moving the radii of imaginary ν_z and ν_r = 1 outwards and inwards respectively. The difference in slope and the somewhat greater deviations at low field are largely due to the measured flutter being lower than calculated at inner radii.

The difference in flutter depends on both radius and coil excitation and is shown in Fig. 9 where the hill minus valley field at several radii is plotted

0018-9499/79/0400-2037$00.75 ©1979 IEEE

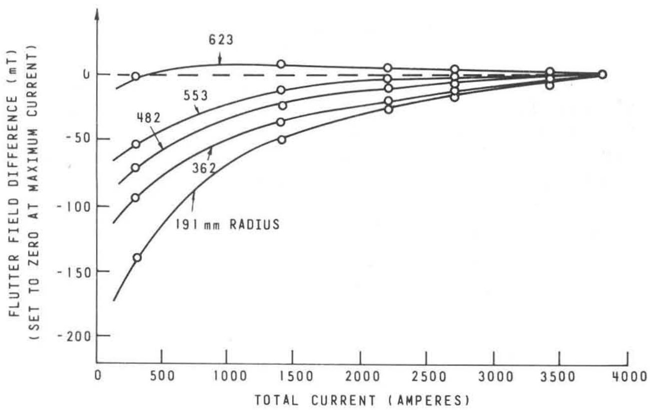

Fig. 9 The change in flutter field (hill minus valley) as a function of the sum of the coil currents for several radii.

against the sum of the coil currents. At low currents the flutter poles are of course not saturated and uniform magnetization is less valid, but at maximum excitation it can be seen that the flutter pole contribution at small radii is still increasing. Over the operating range of the cyclotron the flutter field at 191 mm radius changes by $\sim 2.5\%$ and is lower than calculated at maximum field by $\sim 4\%$. This reduction in flutter at inside radii will reduce the vertical betatron frequency ν_z from 0.13 to 0.12 for 10 MeV/u uranium and from 0.21 to 0.19 for 50 MeV/u carbon which is acceptable.

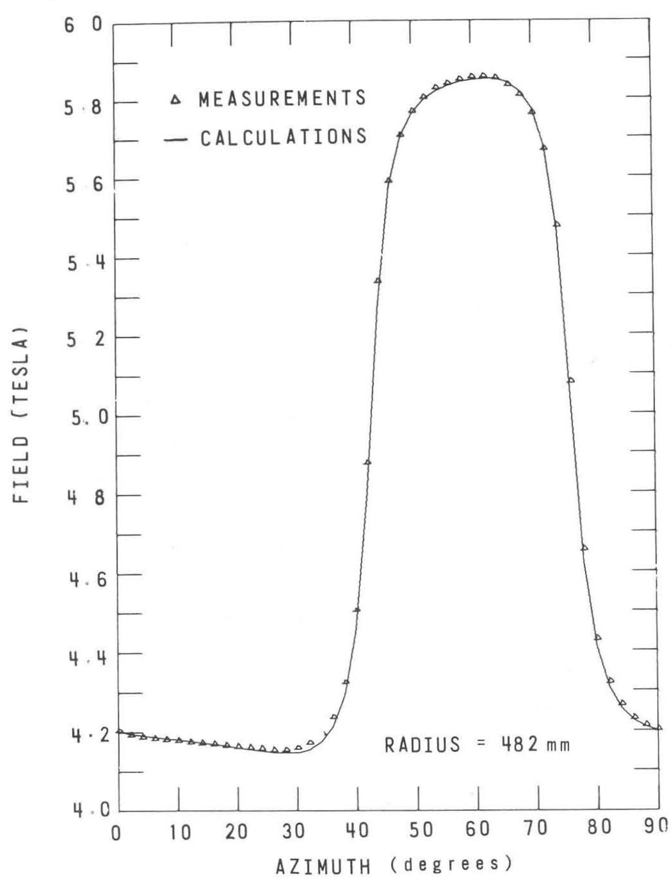

Fig. 10 Measured and calculated azimuthal field profiles at a radius of 482 mm at maximum coil excitation.

In Fig. 10 and 11, the agreement of the measured azimuthal field profiles with calculations is shown for two outer radii where the field exhibits some structure. The asymmetry is produced by the hill spiral. At inner radii the flutter field becomes more sinusoidal.

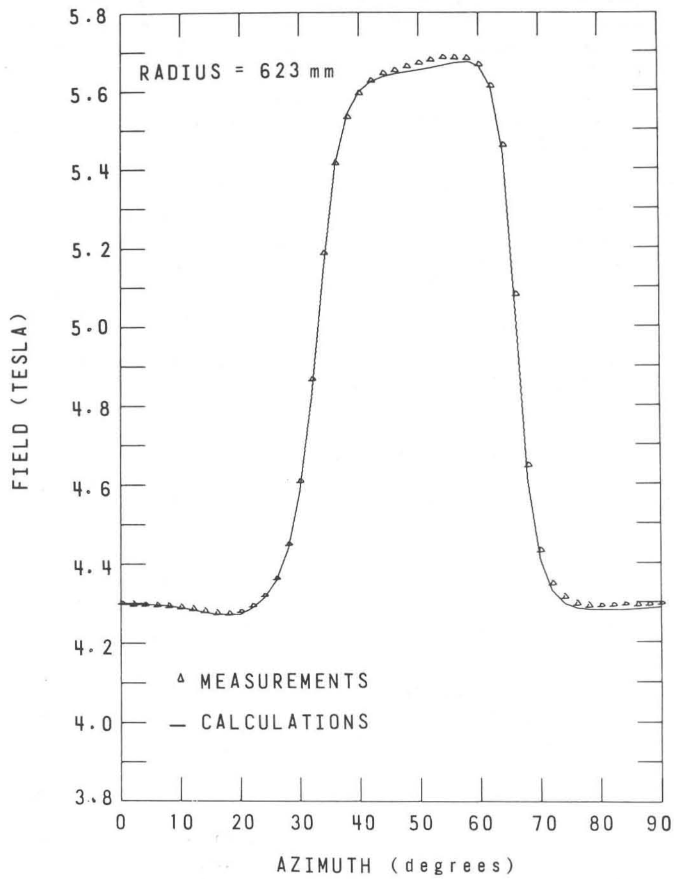

Fig. 11 Measured and calculated azimuthal field profiles at a radius of 623 mm at maximum coil excitation.

The short term (up to several seconds) field stability was measured by a 20-turn coil wrapped around the lower pole near the midplane. With the power supplies in regulation mode, it was more than an order of magnitude better than the required 10^{-5}.

The field measurements also included data on the fields produced by retracting the trim rods. The rods were manually retracted for these tests and the torques required were within 25% of the calculated values. The measured field differences are shown in Fig. 12 and 13 for a 60 mm and 40 mm diameter rod respectively. The data are compared with a TRIM boundary value calculation and a uniform magnetization calculation. The TRIM calculation overestimates the effectiveness of the rods while the uniform magnetization calculation is an underestimate. The agreement in shape and amplitude is clearly enough to ensure the ability of the rods to trim the fields to isochronism as required.

ACKNOWLEDGMENTS

It is a pleasure to acknowledge the able technical assistance of L.F. Birney, K.A. Dobbs, J.J. Hill and A.B. Hood.

0018-9499/79/0400-2038$00.75 ©1979 IEEE

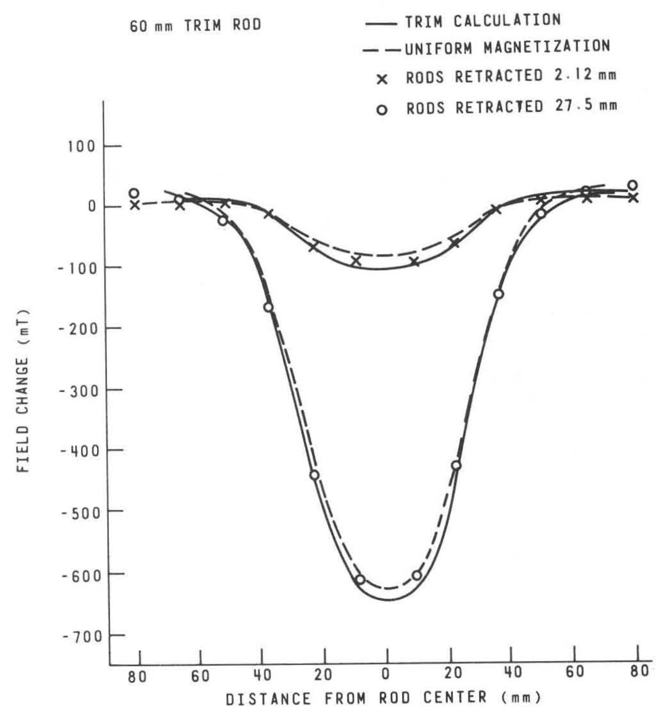

Fig. 12 Measured field profiles for a 60 mm trim rod compared both with a TRIM and a uniform magnetization calculation.

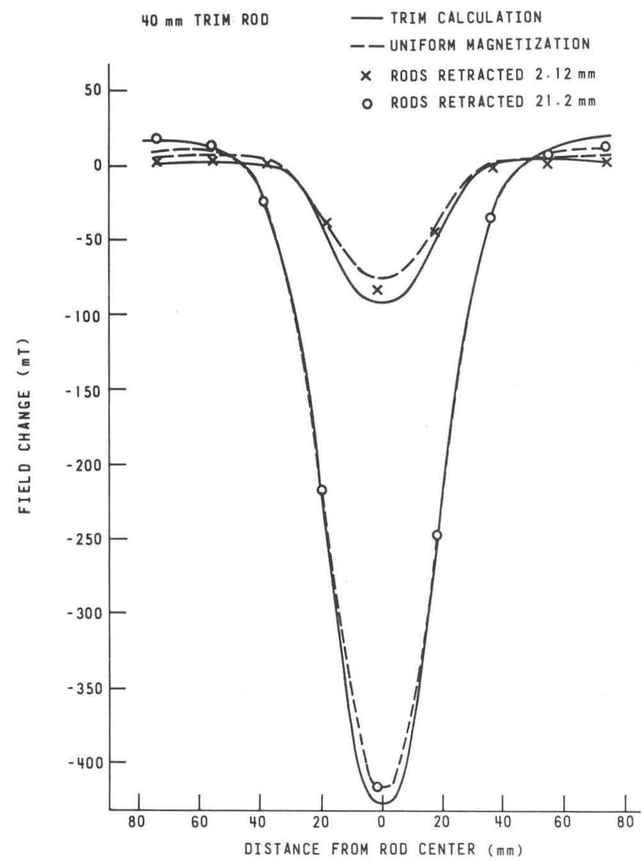

Fig. 13 Measured field profiles for a 40 mm trim rod compared both with a TRIM and a uniform magnetization calculation.

REFERENCES

1. J.H. Ormrod, C.B. Bigham, J.S. Fraser, E.A. Heighway, C.R. Hoffmann, J.A. Hulbert, P.W. James, H.R. Schneider and Q.A. Walker, "Status of the Chalk River Superconducting Heavy-Ion Cyclotron", Proc. IEEE NS-24, 1093 (1977).

2. C.B. Bigham, "The Chalk River Superconducting Heavy-Ion Cyclotron Rf Structure", these proceedings.

3. E.A. Heighway and K.R. Chaplin, "Magnetic Field Related Mechanical Tolerances for the Proposed Chalk River Superconducting Heavy-Ion Cyclotron", Atomic Energy of Canada Limited, Report No. AECL-6079 (1977).

4. D. Güsewell and E.-U. Haebel, "Current Leads for Refrigerator-Cooled Large Superconducting Magnets", Proc. 3rd Int. Cryogenic Engineering Conf., Berlin, 1970, I.P.C. p.187.

5. W. Busse and H. Kluge, "Concept and Status of the Control System for the VICKSI Accelerators at H.M.I. - Berlin", 7th Int. Conf. on Cyclotrons, Zurich, 1975, Birkhäuser, p.557.

6. M.D. Thomason, "Cylindrical Point Coils for Magnetic Field Mapping", Los Alamos report LA-5304-MA (1973).

7. S.W. Mosko, E.D. Hudson, R.S. Lord, D.C. Hensley and J.A. Biggerstaff, "Magnetic Field Measuring System for Remapping the ORIC Magnetic Field", Proc. IEEE NS-24, 1269 (1977).

8. J.S. Colonias, "TRIM: A Magnetostatic Computer Program for the CDC 6600", UCRL-18439 (1968).

** DISCUSSION **

J. REICH: Did you make calculations superposing the trim rod functions to isochronize the field?

J. ORMROD: Yes. The results were reported at the 1977 Particle Accelerator Conference in Chicago.